JOURNAL OF SYNCHROTRON RADIATION

ISSN 1600-5775

Operando X-ray absorption spectroscopy study of the Fischer–Tropsch reaction with a Co catalyst

Chandrani Nayak,[a,b] Preeti Jain,[c] C. P. Vinod,[c] S. N. Jha[a] and D. Bhattacharyya[a]*

[a]Atomic and Molecular Physics Division, Bhabha Atomic Research Centre, Mumbai 400085, India, [b]Homi Bhabha National Institute, Mumbai 400094, India, and [c]Catalysis and Inorganic Chemistry Division, CSIR – National Chemical Laboratory, Dr Homi Bhabha Road, Pune 411008, India. *Correspondence e-mail: dibyendubarc@gmail.com

Received 1 July 2018
Accepted 3 November 2018

Edited by A. F. Craievich, University of São Paulo, Brazil

Keywords: EXAFS; XANES; catalysis; in situ studies; Fischer–Tropsch reaction; structure–activity correlation.

This article describes the setting up of a facility on the energy-scanning EXAFS beamline (BL-09) at RRCAT, Indore, India, for operando studies of structure–activity correlation during a catalytic reaction. The setup was tested by operando X-ray absorption spectroscopy (XAS) studies performed on a Co-based catalyst during the Fischer–Tropsch reaction to obtain information regarding structural changes in the catalyst during the reaction. Simultaneous gas chromatography (GC) measurements during the reaction facilitate monitoring of the product gases, which in turn gives information regarding the activity of the catalyst. The combination of XAS and GC techniques was used to correlate the structural changes with the activity of the catalyst at different reaction temperatures. The oxide catalyst was reduced to the metallic phase by heating at 400°C for 5 h under H_2 at ambient pressure and subsequently the catalytic reaction was studied at four different temperatures of 240, 260, 280 and 320°C. The catalyst was studied for 10 h at 320°C and an attempt has been made to understand the process of its deactivation from the XANES and EXAFS results.

1. Introduction

Studies of structure–activity correlation are essential to understand the performance of catalysts (Weckhuysen, 2002; Hunger & Weitkamp, 2001; Thomas, 1999; Manzoli *et al.*, 2017; Topsøe, 2003) and, in this context, X-ray absorption spectroscopy (XAS) has emerged as an important technique which can give structural information about the catalysts (Newton *et al.*, 2002; Mesu *et al.*, 2005; Tromp *et al.*, 2003). The main advantage of this technique is that it does not need a crystalline sample: it can probe samples in any form, whether crystalline, amorphous, glass, polymer, liquid *etc.*, and therefore can be used as a structure-determining tool for a wide range of homogenous and heterogenous catalysts.

Several ex situ EXAFS experiments have been performed to obtain information about the structure of catalysts, which is then correlated with their catalytic performance. For example, Majeed *et al.* (2015) studied the correlation between the level of Mo dopant and the photocatalytic activity of TiO_2 through EXAFS and photocatalysis studies. Čižmar *et al.* (2017) also studied the correlation between structure and activity of Cu-modified TiO_2–SiO_2 nanoparticles using EXAFS. van Haandel *et al.* (2017) investigated the effect of organic additives on the activity of a (Co)Mo/Al_2O_3 catalyst using EXAFS studies. Many such experiments have been performed where EXAFS studies have given insight into the role of dopants or additives in the catalyst material to improve the catalytic activity, which in turn has helped in designing and fabricating tailor-made catalysts.

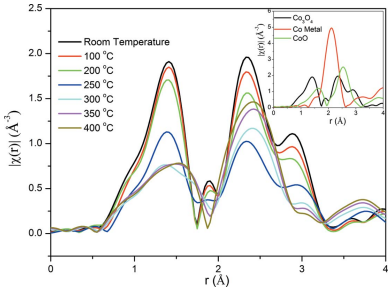

With recent improvements in the performance of synchrotron beamlines and fast data-acquisition systems, an EXAFS spectrum of 1000 eV energy range can now be measured in milliseconds (Müller *et al.*, 2016; Dent, 2002). This experimental revolution heralds a new era of operando measurements where XAS spectra of catalyst samples are recorded during the reaction. Operando measurements have become invaluable in the field of catalysis as they provide exact information during the catalysis process. This has definitely given a better outlook regarding the activity and selectivity of catalysts, and also accurately addresses the problem of deactivation of the catalyst.

Operando EXAFS measurements have been successfully used in many important catalysis systems in the past. For example, Tibiletti *et. al.* (2005) performed in situ EXAFS studies on an oxide-supported gold catalyst during the water gas shift reaction to identify the active species in the catalyst responsible for the reaction. Voronov *et al.* (2014) investigated the Fischer–Tropsch reaction with Co–Re/Al_2O_3 catalysts. Newton *et al.* (2007) investigated Pd catalyst systems during CO/NO cycling. Grunwaldt & Clausen (2002) combined X-ray diffraction (XRD) and EXAFS with online gas analysis and studied Cu-based catalysts for methanol synthesis. Quick EXAFS and Raman measurements have been simultaneously performed for the Fischer–Tropsch reaction with Co/alumina catalysts (Rochet *et al.*, 2013). Newton *et al.* (2004) investigated the behaviour of Rh catalysts in situ during NO reduction by CO with FT–IR, dispersive EXAFS and mass spectrometry.

One of the techniques which is often complemented by time-resolved XAS (TR-XAS) for studying heterogenous catalysis is gas chromatography (GC). Online monitoring of the gaseous species using GC during an operando XAS measurement of a catalyst provides exact information regarding the reaction, which in turn determines the activity of the catalyst, while TR-XAS gives information regarding structural changes within the catalyst. Therefore, a combination of TR-XAS and GC can give insight into the structure–activity correlation of a catalyst system.

The energy-scanning EXAFS beamline (BL-09), Indus-2, RRCAT, Indore, India, has been operational since 2013 (Basu *et al.*, 2014; Poswal *et al.*, 2014) and so far has been used extensively for ex situ XAS measurements on a wide variety of samples. Recently, a continuous-mode EXAFS facility was successfully commissioned on this beamline for fast data acquisition and it has been used to monitor the in situ growth of silver nanopaticles (Poswal *et al.*, 2016). In the present work, we describe the development of an operando XAS measurement setup for studying heterogenous catalysis processes with online gas monitoring using GC at the above beamline with the EXAFS measurements carried out in continuous mode. This setup was used for operando studies of the Fischer–Tropsch reaction using Co_3O_4 nanoparticles supported on the mesoporous silica sieve SBA-15 (Sigma–Aldrich) as catalyst. The reaction was performed in a specially designed cell with a facility for heating and reaction under various gaseous environments. The structure and activity of the catalyst were studied at different reaction temperatures. Deactivation of the catalyst was also investigated in an attempt to find out the factors responsible for this.

Several X-ray-based studies have also been carried out to characterize Co-based catalysts for the Fischer–Tropsch reaction (Herbert *et al.*, 2016). The Co^0 sites are assumed to be the active sites of the catalyst for the Fischer–Tropsch reaction, but there are differences due to the crystal structure of metallic Co. For example, Sadeqzadeh *et al.* (2011) found through in situ XRD/EXAFS measurements that the hexagonal close-packed (h.c.p.) phase of Co is more active than the face-centred cubic (f.c.c.) phase. Also, they reported Co sintering as the main mechanism for catalyst deactivation. Karaca *et al.* (2011) performed in situ XRD measurements on alumina-supported cobalt catalysts promoted with platinum under realistic conditions of the Fischer–Tropsch reaction and found that the formation of a Co_2C phase and Co sintering are the reasons for catalyst deactivation. Similarly, Tsakoumis *et al.* (2012) also performed a combined in situ XAS/powder X-ray diffraction (PXRD) study of a Re-promoted and unpromoted Co catalyst during the Fischer–Tropsch reaction. According to their studies, during the initial deactivation of the catalyst there is no change in the X-ray signal, which suggests that the initial deactivation is a surface-related phenomenon.

2. Experimental details

2.1. Oxide catalyst synthesis

The synthesis of the Co_3O_4 nanoparticles was carried out following the hydrothermal method reported by Dong *et al.* (2007). In a typical synthesis, $Co(CH_3COO)_2{\cdot}4H_2O$ (1 g; Sigma–Aldrich) was dissolved in deionized water (50 ml) with stirring to obtain a transparent solution. Subsequently, 25% NH_3 (5 ml) was added under vigorous stirring and the stirring was continued for 10 min to form a homogenous slurry. The resulting solution was then transferred into a Teflon-lined autoclave which was heated to 150°C for 3 h. Afterwards, the autoclave was allowed to cool down to room temperature naturally and the black precipitate was collected by centrifuge, washed with water and absolute ethanol, and dried at 60°C.

2.2. Preparation of supported Co_3O_4 nanoparticles

A colloidal solution of Co_3O_4 nanoparticles was obtained by dispersing the above precipitate in a minimum amount of water. The desired amount of SBA-15 was added to the colloidal solution of Co_3O_4 nanoparticles to achieve 20 wt% of Co metal loading. The slurry formed was stirred for 2 h, centrifuged, washed with water and ethanol, and dried at 60°C for 12 h. The surface loading of Co in the SBA-15 was checked by X-ray photoelectron spectroscopy measurements (XPS) and found to be slightly less than 20%.

2.3. The Fischer–Tropsch reaction

Chemical production of liquid fuels is one of the alternatives to circumvent the problem of dwindling crude-oil reserves. Fischer–Tropsch synthesis is a good route for the

production of fuel from syngas, which can be obtained from coal, natural gas, biomass *etc.* (Khodakov, 2009). The Fischer–Tropsch (FT) reaction involves hydrogenation of CO to produce hydrocarbons such as alkanes, alkenes, oxygenates *etc.*, as follows.

Paraffins:

$$(2n+1)H_2 + nCO \longrightarrow C_nH_{2n+2} + nH_2O. \quad (1)$$

Olefins:

$$2nH_2 + nCO \longrightarrow C_nH_{2n} + nH_2O. \quad (2)$$

Alcohols:

$$2nH_2 + nCO \longrightarrow C_nH_{2n-1}OH + (n-1)H_2O. \quad (3)$$

A supported cobalt catalyst in the metallic state is the most favourable for FT synthesis at low temperature. In this work, SBA-15-supported Co_3O_4 nanoparticles, synthesized as above, were used for the FT reaction. A small quantity (50 mg) of the as-prepared SBA-15-supported oxide catalyst was pressed into a thin 12 mm-diameter pellet which was used as the sample in a stainless steel cell (described below) for the FT reaction. The oxide catalyst was first reduced by heating it to 400°C at a ramp rate of 10°C min^{-1} under a 20 ml min^{-1} flow of H_2. The temperature of the sample was maintained at 400°C for 5 h to reduce the oxide catalyst to metallic Co. After reduction of the as-prepared catalyst into metallic cobalt, the temperature of the cell was reduced to the reaction temperature in the presence of H_2 and, on attaining the desired temperature, the H_2 gas flow was reduced. The catalytic reaction was subsequently monitored at a few different temperatures, viz. 240, 260, 280 and 320°C, with the syngas in an H_2:CO ratio of 3:1 and with N_2 as internal standard. The flows of the CO, H_2 and N_2 gases were maintained at 2, 6 and 1 ml min^{-1}, respectively, during the catalytic reaction. Structural changes in the catalyst sample during the reaction were studied at the above-mentioned temperatures using in situ XAS.

2.4. In situ reaction cell and gas-flow system

For operando XAS measurements, a stainless steel reaction chamber was used, with Be windows for X-ray transmission. The sample was mounted on a stainless steel block which can be heated with two cartridge heaters, each having a power of 200 W. The window flanges and the top flange of the chamber are water cooled. The temperature of the sample can go up to 400°C. A thermocouple was introduced into the cell from the top flange and fixed at the sample holder, thus touching the sample. The temperature at the sample position was controlled to within ±1°C of the set value using a temperature controller coupled with the power supply of the cartridge heaters. The chamber is provided with two 1/4-inch stainless steel tubes for the inlet and outlet of the reaction gases. The inlet of the reaction chamber is connected to a gas manifold where the three gases can be mixed and then fed into the chamber, and the flow of each gas can be controlled using three separate computer-controlled mass-flow controllers (MFCs) and shut-off valves. The outlet of the reaction chamber is connected to a computer-controlled gas chromatograph (Netel, India) through a six-port auto-sampling valve for the detection of the product gases. The six-port auto-sampling valve has a sample loop of 1 ml and the gas in the sample loop goes to the gas chromatograph for analysis, while the rest of the outgas goes to the vent. The product gases (H_2, N_2, CO and CH_4) are detected using a molecular sieve 5A column and using Ar as the carrier gas for the gas chromatograph. The CO conversion percentage $\%CO_{conv}$ is calculated from the GC data using the following formula (Jalama *et al.*, 2007),

$$\%CO_{conv} = \frac{\left[CO_{(in)} - CO_{(out)} \times \frac{N_{2(in)}}{N_{2(out)}}\right] \times 100}{CO_{(in)}}, \quad (4)$$

where $CO_{(in)}$, $CO_{(out)}$, $N_{2(in)}$ and $N_{2(out)}$ are the concentrations of the CO and N_2 gases at the inlet and outlet of the reaction chamber, respectively, as measured by the gas chromatograph. A schematic diagram of the experimental setup and a photograph of the reaction cell are shown in Fig. 1.

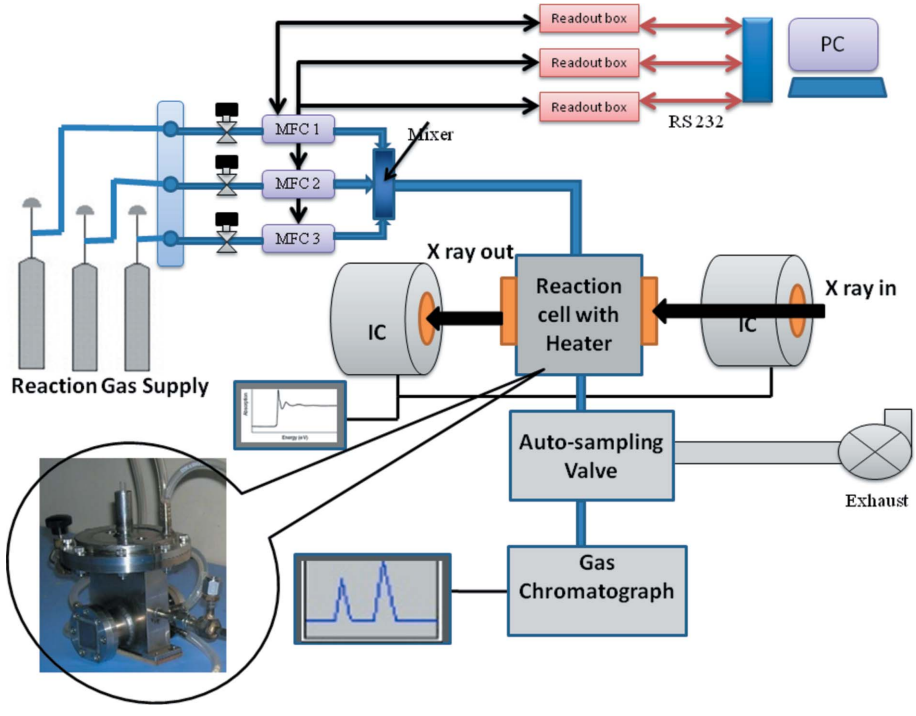

Figure 1
A schematic diagram of the experimental setup, along with a photograph of the reaction cell.

2.5. Operando XAS

Time-resolved XAS measurements on the catalyst sample at the Co *K*-edge were carried out in transmission mode on the scanning EXAFS beamline (BL-9) at the Indus-2 synchrotron source (2.5 GeV, 100 mA). The beamline uses a double-crystal monochromator (DCM) which works in the photon energy range 4–25 keV with a resolution of 10^4 at 10 keV. A 1.5 m horizontal pre-mirror with meridionial cylindrical curvature is used prior to the DCM for collimation of the beam and rejection of higher harmonics. The second crystal of the DCM is a sagittal cylinder with a radius of curvature in the range 1.28–12.91 m, which provides horizontal focusing to the beam, while vertical focusing of the beam is performed by a cylindrical post-mirror mounted facing down. For operando XAS measurements in transmission mode, the reaction chamber containing the sample is placed between two ionization chamber detectors. The first ionization chamber measures the incident flux (I_0), the second ionization chamber measures the transmitted intensity (I_t) and the absorbance of the sample is obtained as $\mu = \exp(-I_t/I_0)$.

For the above measurements the beamline was operated in the recently developed continuous-scan mode which enables time-resolved study on the minute scale while retaining the advantage of high resolution offered by the step-by-step scan of the DCM. This measurement mode is based on restricted movement of the second crystal of the DCM and energy selection is performed by only changing the Bragg angle by simultaneous rotational motion of the two crystals. The details of this measurement scheme have been reported elsewhere (Poswal *et al.*, 2016). In this mode, a full EXAFS scan is taken in 5 min, while XANES data can be acquired in less than 1 min. EXAFS oscillations were extracted from plots of the X-ray absorption spectra $\mu(E)$ versus E, following the standard procedure (Bunker, 2010; Kelly *et al.*, 2008; Konigsberger & Prins, 1988) and using the *IFEFFIT* software package (Newville *et al.*, 1995).

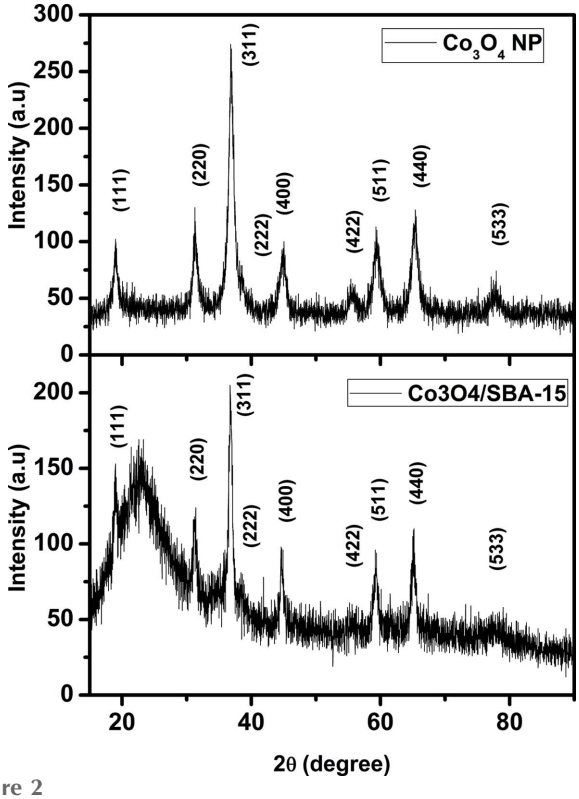

Figure 2
XRD spectra (top) of the as-prepared Co_3O_4 nanoparticles and (bottom) of the Co_3O_4 nanoparticles supported on SBA-15.

3. Results and discussion

Fig. 2 shows the XRD patterns of the as-prepared Co_3O_4 nanoparticles and of the Co_3O_4 nanoparticles supported on SBA-15. Both samples show peaks in the diffraction pattern corresponding to the Co_3O_4 crystal structure. No other phase was detected in the XRD spectra. Figs. 3(*a*) and 3(*b*) show the operando XANES spectra measured during the reduction of the as-prepared oxide catalyst sample, and the inset in Fig. 3(*a*)

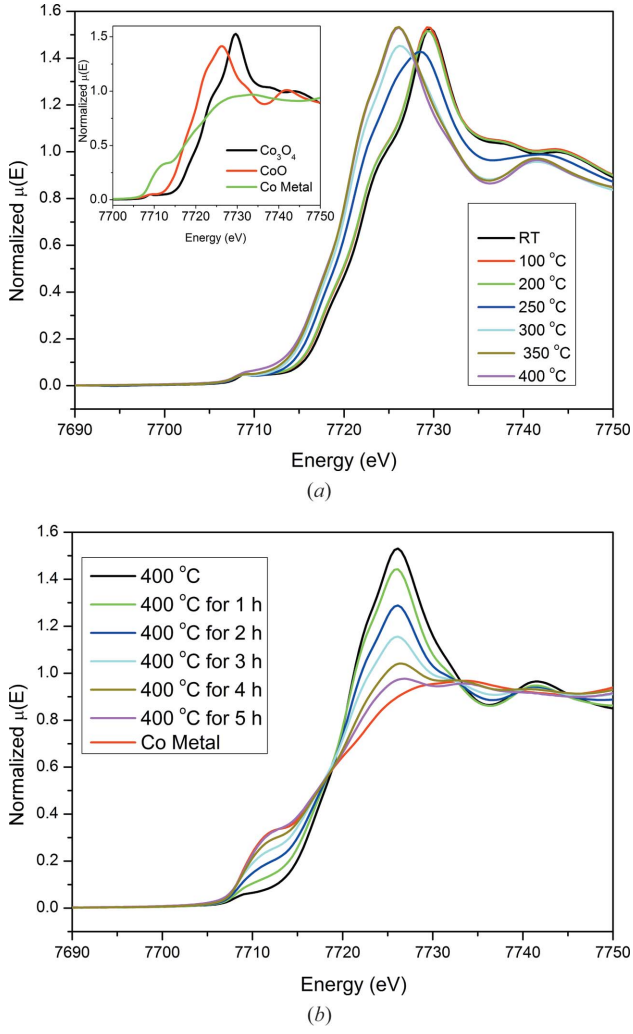

Figure 3
(*a*) In situ XANES spectra recorded at different temperatures during reduction of the as-prepared oxide catalyst sample. (Inset) XANES spectra of the Co standards, *i.e.* Co_3O_4, CoO and Co metal. (*b*) In situ XANES spectra recorded at 400°C at different time intervals during reduction of the as-prepared oxide catalyst sample.

shows the XANES spectra of the Co standards, *i.e.* Co_3O_4, CoO and Co metal. From the figure, it is evident that the XANES features of the as-prepared sample resemble those of Co_3O_4. During reduction at 350°C the spectrum shifts to lower energy, with XANES features resembling those of the CoO spectrum. As the temperature is increased to 400°C, the intensity of the white line decreases and after 5 h of heating at 400°C [Fig. 3(*b*)] the absorption edge matches that of metallic Co foil with reduced intensity of the white line. Therefore, the operando XANES measurements during reduction of the as-prepared sample indicate that, as the temperature is increased, the as-prepared Co_3O_4 catalyst first reduces to CoO and then to metallic Co.

The operando EXAFS spectra recorded during reduction of the as-prepared oxide catalyst sample are shown in Figs. 4(*a*) and 4(*b*). The EXAFS spectrum of the as-prepared sample resembles that of Co_3O_4 [shown in the inset of Fig. 4(*a*)] with a Co—O peak at 1.4 Å and a Co—Co peak at 2.3 Å. As the temperature is increased during reduction of the catalyst, the intensities of both these peaks decrease and the peaks shift towards higher *r* values. This may be due to the formation of CoO during the reduction process, as also seen from analysis of the XANES spectra. As the temperature reaches 400°C, after 1 h a new peak starts to appear near 2 Å which represents the Co—Co bond of metallic Co. At 400°C with increasing time, the intensity of the Co—Co peak at 2 Å increases and the intensities of the other peaks decrease [Fig. 4(*b*)]. After 5 h at 400°C, the EXAFS spectrum has only one prominent peak near 2 Å, which resembles the features of metallic Co as seen from the inset. Therefore, it can be concluded that the sample kept at 400°C for 5 h is completely reduced to metallic Co with no evidence of CoO or Co_3O_4 phases in the EXAFS and XANES spectra. The formation of CoO during hydrogen activation of Co_3O_4 catalyst has also been reported by other researchers (Jacobs *et al.*, 2004; Passos *et al.*, 2017; Rochet *et al.*, 2013).

The reduced sample was then exposed to the reactant gases and the structural changes during the reaction were studied. Fig. 5 shows the changes in the radial distribution function of the catalyst sample undergoing reaction at different temperatures. From this figure, it is evident that at 240°C and 260°C the structure of the catalyst does not change. The variation in peak intensity is due to the temperature effect of the disorder factor (σ^2). At 280°C the Co—Co peak near 2 Å shows some variation with time as the reaction proceeds. However, there is no evidence for the appearance of a Co—O peak even at this temperature, which demonstrates that CoO is not formed. The variation in Co—Co peak intensity may be due to disorder in the catalyst system which originates because the activity of the sample increases significantly with temperature.

Fig. 6 shows the percentage of CO conversion at 280°C for 7 h and at 320°C for 10 h. It is seen in this figure that, when the temperature is increased from 280 to 320°C, there is a drastic increase in the CO conversion from 20 to 54%. The CO conversion percentage remains almost constant for 7 h at

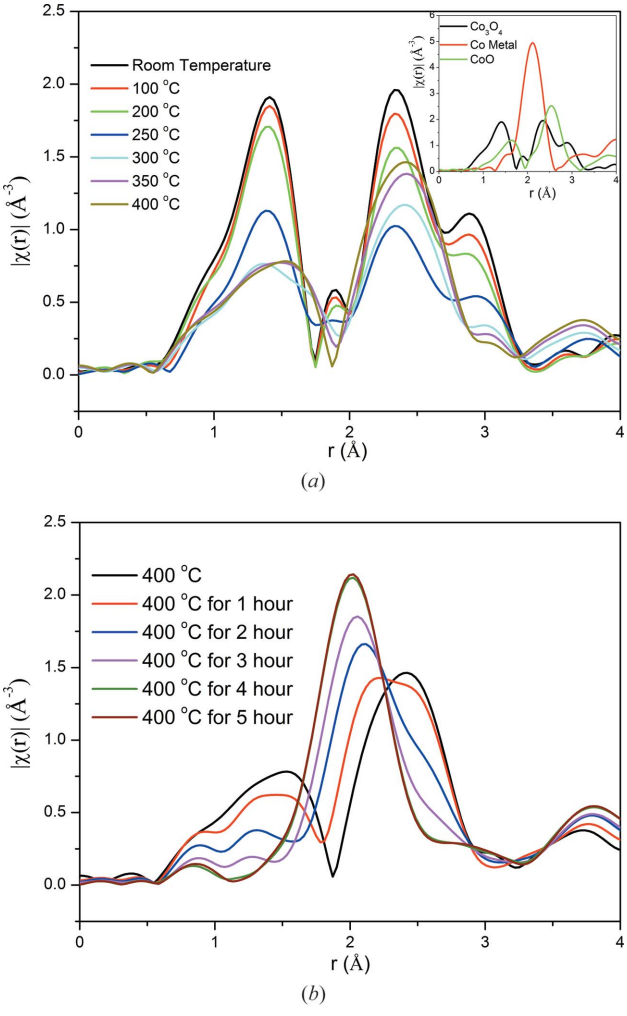

Figure 4
(*a*) In situ EXAFS spectra recorded at different temperatures during reduction of the as-prepared oxide catalyst sample. (Inset) EXAFS spectra of the Co standards, *i.e.* Co_3O_4, CoO and Co metal. (*b*) In situ EXAFS spectra recorded at 400°C at different time intervals during reduction of the as-prepared oxide catalyst sample.

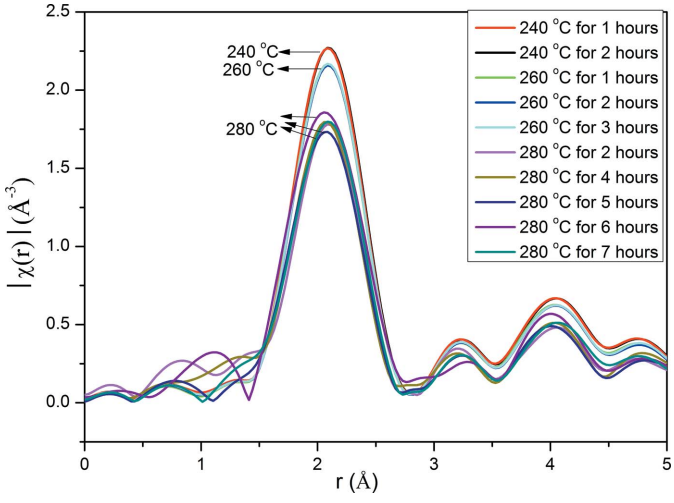

Figure 5
The variation in the EXAFS radial distribution function of the catalyst sample undergoing FT reaction at different temperatures.

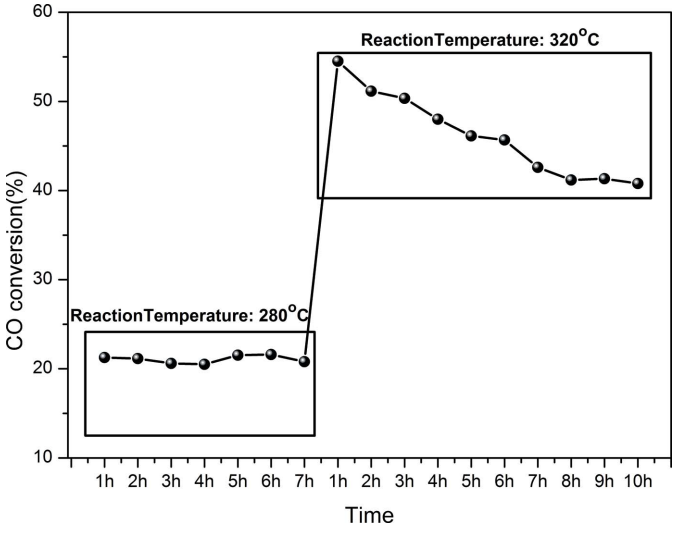

Figure 6
The CO conversion percentage at 280 and at 320°C with time.

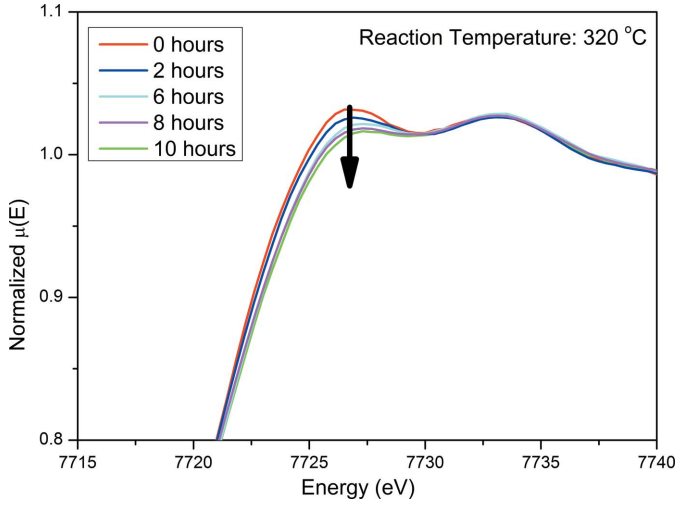

Figure 8
In situ XANES spectra recorded during deactivation of the catalyst at 320°C.

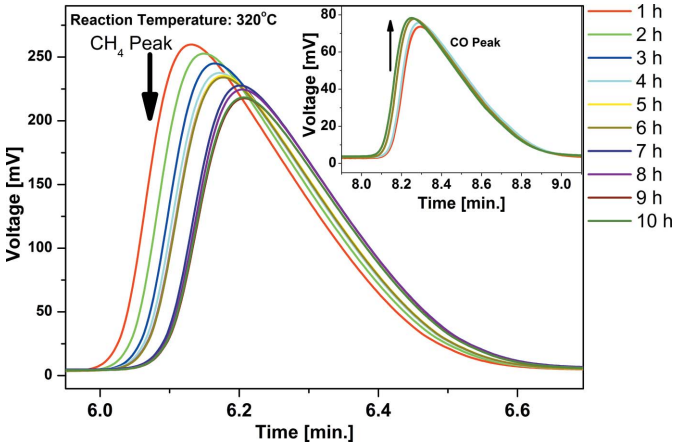

Figure 7
GC data showing the variation in the methane peak intensity. (Inset) GC data showing the variation in the CO peak intensity.

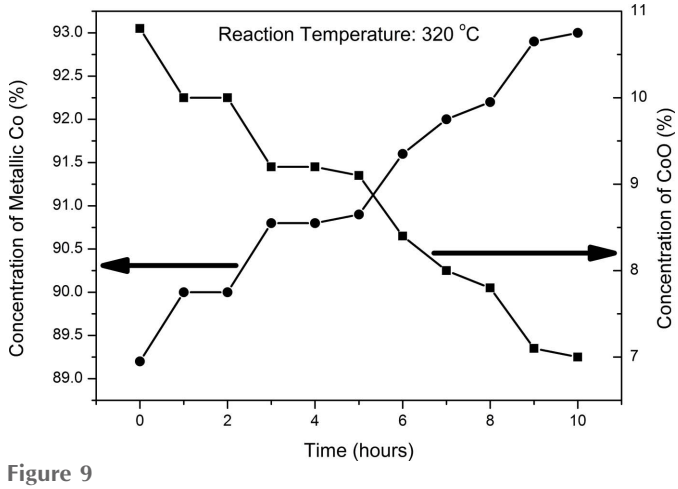

Figure 9
The results of linear combination fitting of the in situ XANES spectra recorded during deactivation of the catalyst at 320°C, with metallic Co and CoO as standards.

280°C, but it decreases monotonically with time from 54 to 41% at 320°C. The intensities of the methane and CO peaks in the GC data decrease and increase, respectively, with time at 320°C, as shown in Fig. 7. This suggests that there is a decline in the performance of the catalyst at 320°C, or in other words the catalyst is deactivating.

Fig. 8 shows the XANES spectra recorded during deactivation of the catalyst at 320°C, which show a decrease in the white line intensity at 7726 eV with time. This suggests further reduction of the catalyst due to the reaction gases. Linear combination fitting (LCF) of the XANES spectra with metallic Co and CoO as standards was performed in the energy range of −20 eV to 30 eV around the absorption edge of the normalized μ spectra. The values of the LCF weights were restricted between 0 and 1, and the sum of all the weights was also constrained to 1. The R factors of the LCFs are less than 0.004. From the results of the LCF (Fig. 9), it can be observed that the metallic Co percentage increases and the CoO percentage decreases with time as the reaction proceeds at 320°C. This observation rules out the possibility of formation of CoO during the reaction which might act as a contributing factor for deactivation. The EXAFS spectra (Fig. 10) resemble that of metallic Co and the intensity of the Co—Co peak near 2 Å increases with time. There is no evidence of Co—O bonds in the EXAFS spectra. Therefore, the EXAFS results corroborate the XANES analysis results, confirming that no CoO phase is formed during deactivation of the catalyst.

Many researchers have tried to find out the reason for deactivation of Co-based catalysts in the FT reaction. Rochet *et al.* (2013) found that the Co catalyst deactivates due to reoxidation of the catalyst in the presence of the water produced in the FT reaction, but this is ruled out in the present case from the above observation. Another common cause of deactivation of catalysts is sintering, *i.e.* an increase in particle size during reaction (DeLaRiva *et al.*, 2013) leading to a loss of surface area and hence deactivation. However, sintering generally leads to an increase in the intensity of the metal–

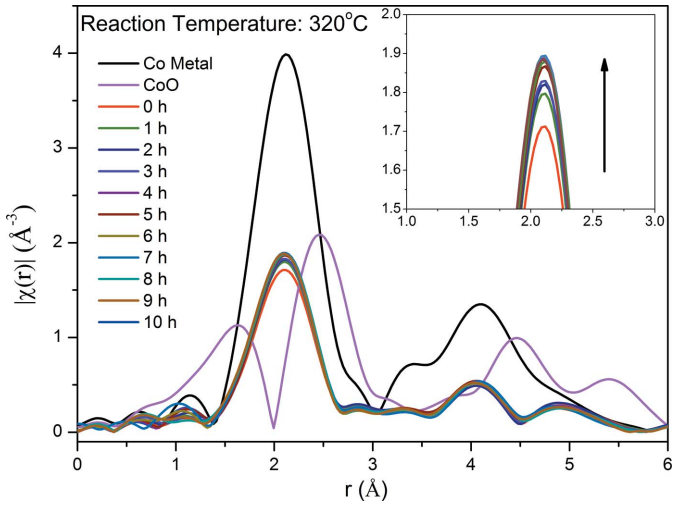

Figure 10
In situ EXAFS spectra recorded during deactivation of the catalyst at 320°C. (Inset) An enlarged view of the peaks at 2 Å.

metal peak in the FT EXAFS spectra and hence in coordination number (Grunwaldt & Clausen, 2002). The experimental EXAFS spectra of the present catalyst sample during deactivation of the catalyst at 320°C were fitted from 1.5 to 3 Å assuming a Co—Co shell at 2.50 Å and having a coordination number of 12 (not shown here) and the fitting results are tabulated in Table 1. From the EXAFS fitting results it can be inferred that the Co—Co bond length does not change with time during deactivation of the catalyst at 320°C. There is an increase in the Co—Co coordination number with time during deactivation of the catalyst at 320°C, but the change is not significant and it is comparable with the error limits of ±10%. Hence, it may not imply any sintering of the catalyst during the reaction. Also, the increase in coordination number may be due to an increase in the proportion of metallic Co phase in the catalyst, as determined from the LCF of the XANES spectra (Fig. 9).

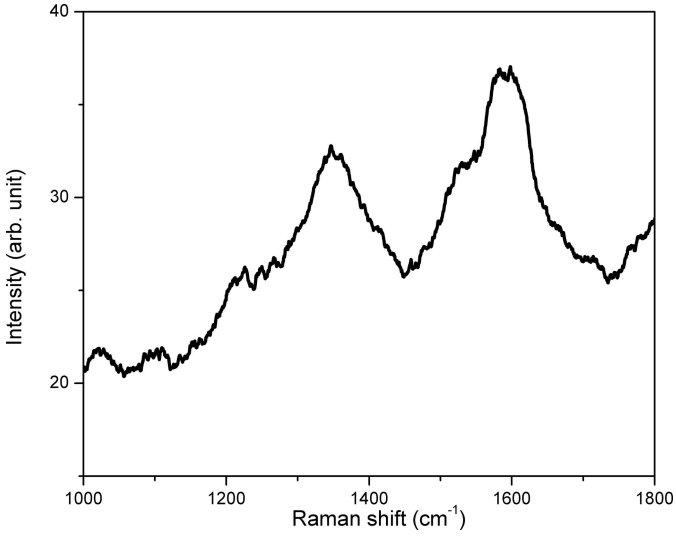

Figure 11
The ex situ Raman spectrum of the deactivated catalyst sample.

Table 1
Co *K*-edge EXAFS fitting results during deactivation of the catalyst at 320°C.

	Co—Co path		
Time (h)	*r* (Å)	*N*	σ^2 (Å^2)
0	2.46 ± 0.01	9.1 ± 1.4	0.0113 ± 0.0017
1	2.46 ± 0.01	9.6 ± 1.2	0.0115 ± 0.0015
2	2.46 ± 0.01	9.9 ± 1.4	0.0116 ± 0.0016
3	2.46 ± 0.01	10.0 ± 1.2	0.0117 ± 0.0014
4	2.46 ± 0.01	9.9 ± 1.0	0.0113 ± 0.0012
5	2.46 ± 0.01	10.0 ± 1.0	0.0116 ± 0.0012
6	2.46 ± 0.01	10.1 ± 0.9	0.0114 ± 0.0013
7	2.46 ± 0.01	10.1 ± 1.0	0.0113 ± 0.0011
8	2.46 ± 0.01	10.2 ± 1.0	0.0122 ± 0.0012
9	2.46 ± 0.01	9.7 ± 0.8	0.0108 ± 0.0011
10	2.46 ± 0.01	10.1 ± 0.9	0.0116 ± 0.0011

Passos *et al.* (2014, 2017) have studied Co-based catalysts for ethanol steam reforming reactions. They observed that CoO enables cleaning of the catalyst surface by oxidation of deposited carbon, and a very low Co^{+2}/Co ratio in the catalyst sample leads to deactivation of the catalyst due to surface carbon deposition. Under FT reaction conditions, many reactions occur. One of these is the Boudouard reaction,

$$CO + CO \longrightarrow C + CO_2, \quad (5)$$

which may lead to the formation of carbon.

In our case, the percentage of Co^{2+} in the activated catalyst is also low (around 11%) and there is no further increase in the percentage of Co^{2+} due to reoxidation during deactivation. Therefore, the process of deactivation may be attributed to carbon formation on the surface of the catalyst during the reaction which does not get removed due to the low concentration of CoO species in the sample. This has also been confirmed through Raman spectroscopic measurements on the deactivated catalyst. The Raman spectrum of the deactivated catalyst is shown in Fig. 11, which gives two broad peaks typical of coke deposits. Similar spectra were observed by Passos *et al.* (2017) on spent catalysts of ethanol steam reforming reactions after deactivation due to surface carbon deposits. It should be mentioned here that Moodley *et al.* (2009) also identified carbon deposition as one of the deactivation mechanisms of cobalt-based FT synthesis catalysts by characterizing the spent catalyst using both surface characterization techniques like X-ray photoelectron spectroscopy and bulk characterization tools like temperature-programmed (TPO/TPH) techniques and transmission electron microscopy.

4. Conclusions

A facility has been set up on the energy-scanning EXAFS beamline (BL-09) at RRCAT, Indore, India, for operando studies of structure–activity correlation during catalytic reactions using simultaneous measurements of X-ray absorption spectroscopy (XAS) and gas chromatography. XAS provides information regarding structural changes in the catalyst during the reaction, while gas chromatography monitors the product

gases of the reaction, which in turn gives information regarding the activity of the catalyst.

Using this facility, SBA-15-supported Co_3O_4 nanoparticle catalysts were studied in situ during the Fischer–Tropsch reaction for methane generation by the reaction of CO and H_2. The catalyst was first reduced by heating it at 400°C for 5 h under H_2 at ambient pressure and it was found from XANES measurements that the as-prepared catalyst first reduces to CoO and then to metallic Co during reduction.

The activity of the reduced catalyst was subsequently observed at a few different temperatures, viz. 240, 260, 280 and 320°C, and it was found by XANES and EXAFS measurements that the structure of the catalyst does not show any significant change during the Fischer–Tropsch reaction at these temperatures and remains in the metallic Co phase.

It has further been observed that, as the reaction temperature is increased from 280 to 320°C, the activity of the catalyst increases significantly. However, at 320°C the Co catalyst shows deactivation with time. The catalyst was studied for 10 h at 320°C and an attempt was made to understand the process of deactivation using XANES and EXAFS analysis.

From the structural analysis results it was observed that there is no evidence of formation of a CoO phase during the reaction which might be responsible for deactivation of the catalyst. There is also no clear evidence from the XAS measurements of any sintering of the catalyst during the reaction. Therefore, there is a strong possibility that deactivation of the catalyst is caused by carbon formation on the surface of the catalyst which does not get removed because of the very low concentration of CoO in the reduced sample. This was confirmed by ex situ Raman spectroscopy measurements on the deactivated catalyst.

References

Basu, S., Nayak, C., Yadav, A. K., Agrawal, A., Poswal, A. K., Bhattacharyya, D., Jha, S. N. & Sahoo, N. K. (2014). *J. Phys. Conf. Ser.* **493**, 012032.

Bunker, G. (2010). *Introduction to XAFS: A Practical Guide to X-ray Absorption Fine Structure Spectroscopy*. Cambridge University Press.

Čižmar, T., Štangar, U. & Arčon, I. (2017). *Catal. Today*, **287**, 155–160.

DeLaRiva, A. T., Hansen, T. W., Challa, S. R. & Datye, A. K. (2013). *J. Catal.* **308**, 291–305.

Dent, A. J. (2002). *Top. Catal.* **18**, 27–35.

Dong, Y., He, K., Yin, L. & Zhang, A. (2007). *Nanotechnology*, **18**, 435602.

Grunwaldt, J. D. & Clausen, B. S. (2002). *Top. Catal.* **18**, 37–43.

Haandel, L. van, Bremmer, G. M., Hensen, E. J. M. & Weber, Th. (2017). *J. Catal.* **351**, 95–106.

Herbert, J. J., Senecal, P., Martin, D. J., Bras, W., Beaumont, S. K. & Beale, A. M. (2016). *Catal. Sci. Technol.* **6**, 5773–5791.

Hunger, M. & Weitkamp, J. (2001). *Angew. Chem. Int. Ed.* **40**, 2954–2971.

Jacobs, G., Chaney, J. A., Patterson, P. M., Das, T. K. & Davis, B. H. (2004). *Appl. Catal. Gen.* **264**, 203–212.

Jalama, K., Coville, N., Hildebrandt, D., Glasser, D., Jewell, L., Anderson, J., Taylor, S., Enache, D. & Hutchings, G. (2007). *Top. Catal.* **44**, 129–136.

Karaca, H., Safonova, O. V., Chambrey, S., Fongarland, P., Roussel, P., Griboval-Constant, A., Lacroix, M. & Khodakov, A. Y. (2011). *J. Catal.* **277**, 14–26.

Kelly, S. D., Hesterberg, D. & Ravel, B. (2008). *Analysis of Soils and Minerals using X-ray Absorption Spectroscopy. Methods of Soil Analysis*, Part 5, *Mineralogical Methods*, edited by A. L. Ulery & R. Drees, pp. 387–464. Madison, Wisconsin, USA: Soil Science Society of America.

Khodakov, A. Y. (2009). *Catal. Today*, **144**, 251–257.

Konigsberger, D. C. & Prins, R. (1988). *X-ray Absorption: Principles, Applications, Techniques of EXAFS, SEXAFS and XANES*. New York: Wiley.

Majeed, J., Nayak, C., Jha, S. N., Bhattacharyya, K., Bhattacharyya, D. & Tripathi, A. K. (2015). *RSC Adv.* **5**, 90932–90940.

Manzoli, M., Vindigni, F., Tabakova, T., Lamberti, C., Dimitrov, D., Ivanov, K. & Agostini, G. (2017). *J. Mater. Chem. A*, **5**, 2083–2094.

Mesu, J., van der Eerden, A. M. J., de Groot, F. M. F. & Weckhuysen, B. M. (2005). *J. Phys. Chem. B*, **109**, 4042–4047.

Moodley, D. J., van de Loosdrecht, J., Saib, A. M., Overett, M. J., Datye, A. K. & Niemantsverdriet, J. W. (2009). *Appl. Catal. Gen.* **354**, 102–110.

Müller, O., Nachtegaal, M., Just, J., Lützenkirchen-Hecht, D. & Frahm, R. (2016). *J. Synchrotron Rad.* **23**, 260–266.

Newton, M. A., Belver-Coldeira, C., Martínez-Arias, A. & Fernández-García, M. (2007). *Nat. Mater.* **6**, 528–532.

Newton, M. A., Dent, A. J. & Evans, J. (2002). *Chem. Soc. Rev.* **31**, 83–95.

Newton, M. A., Jyoti, B., Dent, A. J., Fiddy, S. G. & Evans, J. (2004). *Chem. Commun.* pp. 2382–2383.

Newville, M., Ravel, B., Haskel, D., Rehr, J. J., Stern, E. A. & Yacoby, Y. (1995). *Physica B*, **154**, 208.

Passos, A. R., Martins, L., Pulcinelli, S. H., Santilli, C. V. & Briois, V. (2014). *Catal. Today*, **229**, 88–94.

Passos, A. R., Martins, L., Pulcinelli, S. H., Santilli, C. V. & Briois, V. (2017). *ChemCatChem*, **9**, 3918–3929.

Poswal, A. K., Agrawal, A., Poswal, H. K., Bhattacharyya, D., Jha, S. N. & Sahoo, N. K. (2016). *J. Synchrotron Rad.* **23**, 1518–1525.

Poswal, A. K., Agrawal, A., Yadav, A. K., Nayak, C., Basu, S., Kane, S. R., Garg, C. K., Bhattachryya, D., Jha, S. N. & Sahoo, N. K. (2014). *AIP Conf. Proc.* **159**, 649–651.

Rochet, A., Moizan, V., Diehl, F., Pichon, C. & Briois, V. (2013). *Catal. Today*, **205**, 94–100.

Sadeqzadeh, M., Karaca, H., Safonova, O. V., Fongarland, P., Chambrey, S., Roussel, P., Griboval-Constant, A., Lacroix, M., Curulla-Ferré, D., Luck, F. & Khodakov, A. Y. (2011). *Catal. Today*, **164**, 62–67.

Thomas, J. M. (1999). *Angew. Chem. Int. Ed.* **38**, 3588–3628.

Tibiletti, D., Fonseca, A. A., Burch, R., Chen, Y., Fisher, J. M., Goguet, A., Hardacre, C., Hu, P. & Thompsett, D. (2005). *J. Phys. Chem. B*, **109**, 22553–22559.

Topsøe, H. (2003). *J. Catal.* **216**, 155–164.

Tromp, M., Sietsma, J. R. A., van Bokhoven, J. A., van Strijdonck, G. P. F., van Haaren, R. J., van der Eerden, A. M. J., van Leeuwen, P. W. N. M. & Koningsberger, D. C. (2003). *Chem. Commun.* pp. 128–129.

Tsakoumis, N. E., Voronov, A., Rønning, M., van Beek, W., Borg, Ø., Rytter, E. & Holmen, A. (2012). *J. Catal.* **291**, 138–148.

Voronov, A., Tsakoumis, N. E., Hammer, N., van Beek, W., Emerich, H. & Rønning, M. (2014). *Catal. Today*, **229**, 23–33.

Weckhuysen, B. M. (2002). *Chem. Commun.* pp. 97–110.